Heat and Mass Transfer (2022) 58:1247–1262
https://doi.org/10.1007/s00231-021-03172-0

ORIGINAL ARTICLE

Research on the heat transfer characteristics of air-atomized water spray cooling by experiment and inverse heat conduction method

Lidan Ning[1] · Shuncun Luo[1] · Zhichao Li[1] · Lianfang He[1] · Huiping Li[1]

Received: 14 May 2021 / Accepted: 13 December 2021 / Published online: 3 February 2022

Abstract

The heat transfer characteristics of air-atomized water spray cooling on the hot metallic surface are presented and discussed in this paper. The controlling parameters mainly investigated are air pressure and spray height. The effects of these parameters on the important thermal characteristics such as interfacial heat transfer coefficient, cooling rate, and wetting layer evolution attained by experiment and inverse heat conduction method. The value of interfacial heat transfer coefficient is proportional to the air pressure and inversely proportional to the spray height. As the air pressure is 0.2 MPa, and the spray height is 40 mm, the maximum cooling rate is 85.08 ℃/s. There is no film boiling stage under this condition. At the spray height is 80 mm, and air pressure is 0.3 MPa, the maximum cooling rate is 62.6 ℃/s. In addition, transition boiling and nucleate boiling always exist, but their retention time is different under different conditions. The temperature-dependent interfacial heat transfer mechanism of air-atomized water spray cooling is explored according to the thermal characteristics and photographs taken by the high-speed camera. The results show that air pressure and spray height both have an influence on the interfacial heat transfer.

List of symbols

T	Temperature (℃)
ρ	Density (kg/m^3)
c_ρ	Specific heat capacity (J/(kg °C))
λ	Thermal conductivity (W/(m°C))
t	Time (s)
z	The coordinate along the axial direction of the sample
q	Surface heat flux (W/m2)
H	Interfacial heat transfer coefficient (W/(m2·℃))
T_f	The temperature of air-atomized water spraying (°C)

Nomenclature

IHTC	Interfacial heat transfer coefficient
HTC	Heat transfer coefficient
IHCM	Inverse heat conduction method
IHTC	Temperature-dependent interfacial heat transfer coefficient
LFP	Leidenfrost Point
CHF	Critical heat flux

✉ Huiping Li
lihuiping99@163.com

[1] School of Materials Science and Engineering, Shandong University of Science and Technology, 579 Qianwangang Road, Qingdao, Shandong 266510, PR China

1 Introduction

Many experimental and theoretical work on the water jet and spray cooling of hot metallic surface have been carried out by different researchers [1–6]. However, the conventional cooling methodologies used in the metallurgical industries are not appropriate for the production of some specific materials because of the requirement of high cooling rate at elevated temperatures [7].

The cooling methods in the hot working process of metal materials include natural convection cooling, forced convection cooling, boiling heat transfer cooling, etc. The interfacial heat transfer coefficient (IHTC) is usually used to characterize the heat transfer performance and cooling efficiency of different cooling methods. The IHTC of water spray cooling is the highest [8], the heat transfer capacity is the strongest, and the cooling speed of the parts is the fastest. It has been observed that the air-atomized water spray cooling is the most effective cooling method compared to the other methods [9–11]. Future challenges for the advanced cooling technology in industry require a better understanding of the spray cooling phenomenon[12].

In order to understand the heat transfer principles during the spray cooling, it has been shown by many authors that local behavior of spraying droplets contacting with the target surface needs to be analyzed. Das et al. [3] investigated the effect of dextrose added high mass flux spray cooling on

heat transfer rate by using a full cone high mass flux spray nozzle. Captured the whole experiment using a high-speed camera, and the thermal analysis was performed by using an inverse heat conduction algorithm for the prediction of surface heat flux and temperature. S.K. Nayak [10] reported results of experimental investigation on thermal characteristics of spray cooling of hot steel plate under controlled parametric conditions. The heat transfer coefficient (HTC) and heat transfer rates were determined for different water flow rates, nozzle heights, and plate thicknesses. Zhao et al. [13] conducted experiments with the different levels of subcooling, heat flux input, inlet pressure and nozzle-to-surface distance, and video image of the surface spray performance were recorded by a high speed camera. Chakraborty et al. [14] performed extensive spray cooling experiments on a 6 mm thick hot stainless steel plate (> 900 ℃). High speed photography was used at a lower temperature to visualize a single droplet impact and to understand the effect of surface tension and underlying physics on the heat transfer phenomenon.

During the spray cooling process, it is essential to remove heat efficiently and uniformly without cracking or distorting the slab. It is challenging to obtain an accurate HTC on the surface of the slab and employ the obtained HTC as the boundary condition of the solidification calculation [15]. R. Dou [16] carried out experiments for full cone water spray cooling on a metal plate with high temperature at different water pressure levels. The heat flux is obtained by solving a 1D inverse heat conduction problem and the accuracy of the heat flux is verified by 3D heat conduction analysis. Zhang et al. [17] performed transient experiments to analyze the spray cooling of high-temperature stainless steel (SUS304) using a commercial flat pattern air-atomized spray nozzle and the surface heat flux was calculated by the inverse heat conduction problem. Chabicovsky et al. [6] studied the spray cooling starting at surface temperatures of about 1200 ℃ and finishing at the Leidenfrost temperature, and used one-dimensional sequential Beck's approach [18, 19] to calculate the heat fluxes, the surface temperatures and IHTC. Hadała et al. [20] investigated the water–air assisted spray cooling of vertical plates, and a model of local HTC as function of pressure, surface temperature and distance from stagnation point based on a large set of HTC has been developed.

Overviewing the previous literature, it can be summarized in Table 1 from the perspectives of spray pressure, spray height, wetting front propagation and calculation of IHTC by inverse heat conduction method (IHCM). Few studies have reported the thermal characteristics of air-atomized water spray cooling of hot metallic surface in conjunction with the IHTC attained by the IHCM and the wetting front propagation. It is difficult to understand the heat removal phenomena.

In this paper, transient experiments were performed to analyze spray cooling of stainless steel at elevated temperature under different conditions using an air-assisted atomizer. The controlling parameters mainly investigated in this paper were the air pressure (0.1—0.3 MPa), spray height (40—120 mm) from the target surface. The effects of these parameters on the important thermal characteristics such as HTC, cooling rates, and wetting front movement were measured and examined. IHCM was used to calculate the surface temperature, IHTC. The LFP is determined according to the wetting layer evolution and surface temperature, IHTC, and heat flux. The temperature-dependent interfacial heat transfer mechanism of air-atomized water spray cooling is explored according to the wetting front propagation taken by a high-speed camera and the transient heat transfer parameters. It has been proved that spray cooling has excellent heat transfer performance due to the rapid evaporation of droplets and liquid film. The surface temperature and the IHTC calculated by the IHCM can provide theoretical guidance for the heat treatment process.

Table 1 Previous investigations on spray cooling

Reference	Spray pressure	Spray height (mm)	Wetting front propagation	Calculation of IHTC by IHCM
Chabicovsky et al. [6]	Water: 11 L/min, 6 L/min; Air pressure: 0.5 bar, 1.5 bar, 3.0 bar	250	No	Yes (Beck's approach)
Nayak and Mishra [10]	Water and air: 0.0 bar to 4.0 bar	120, 180, 240	Yes	No
Dou [16]	Water: 0.2 MPa, 0.3 MPa, 0.5 MPa, 0.7 MPa	250	No	Yes(Levenberg–Marquardt)
Zhang et al. [17]	Water: 0.2–2 MPa Air: constant pressure	170	No	Yes
Hadała et al. [20]	Water pressure: 0.1 MPa, 0.25 MPa, 0.4 MPa	120	No	Yes (FEM)
Chakraborty et al. [14]	Coolant pressure: 4 bar	40, 50, 60, 70, 80	No	Yes

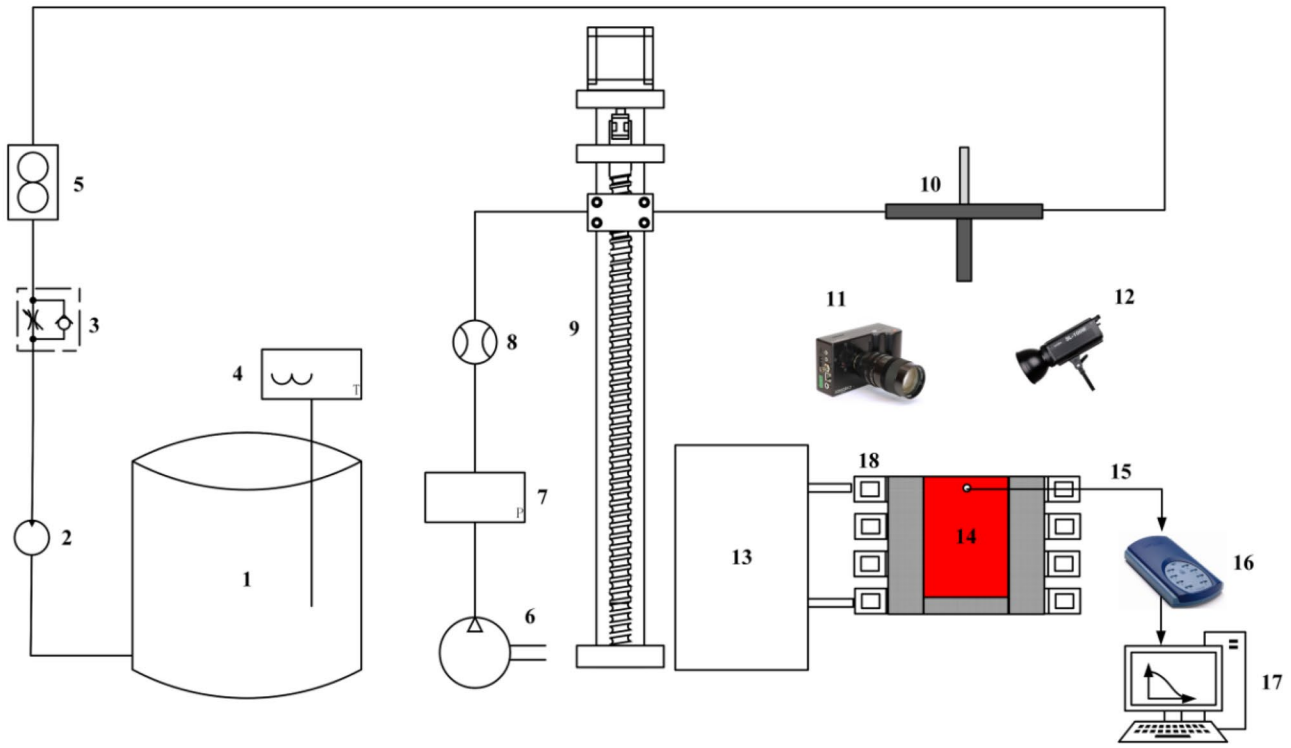

Fig. 1 Schematic of spray cooling setup: 1—water storage tank, 2—water pump, 3—one-way throttle valve, 4—thermometer, 5—flow meter, 6—air compressor, 7—pressure gauge, 8—flow meter, 9—slideway, 10—atomizer, 11—high-speed camera, 12—LED video light, 13—IGBT induction heater, 14—sample, 15—thermocouple, 16—TC-08, 17—computer, 18—inductor

2 Experimental procedures

2.1 Spray cooling system

The experimental system of spray cooling is schematically shown in Fig. 1. It mainly includes coolant supply system, heating system and data acquisition system.

The coolant supply system consists of water reservoir, check valve, flow meter, air compressor and pressure gauge. Air and purified water are chosen as the coolant in the experiment. An air-assisted internally mixed atomizer is used to generate the air-atomized water spray. The atomizer is shown in Fig. 2. Compressed air is supplied by an air compressor, and the pressure used in the experiment is in the range of 0.1—0.3 MPa. The temperature of purified water is approximately 25 ℃. The water flow can be controlled by regulating the air pressure or the control valve of atomizer.

The heating system consists of an insulated gate bipolar transistor (IGBT) induction heating power supply, inductor and sample. IGBT induction heating power supply adopts advanced temperature control technology to realize rapid temperature rise and uniform heating. The sample used in the experiments is 304 stainless steel cylinders with the diameter of 20 mm and the length of 30 mm. The stainless-steel cylinders have a density of 7920 kg/m^3. The diameter of the temperature measuring hole is 1.5 mm. The center line of the temperature measuring hole is 2 mm away from the cooling surface of the sample, as shown in Fig. 3. Current frequency used in the experiment is about 6680 Hz, the IGBT induction heating

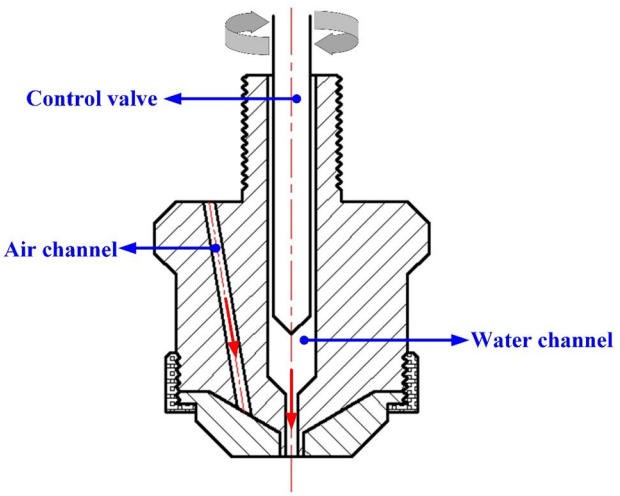

Fig. 2 Schematic of the atomizer

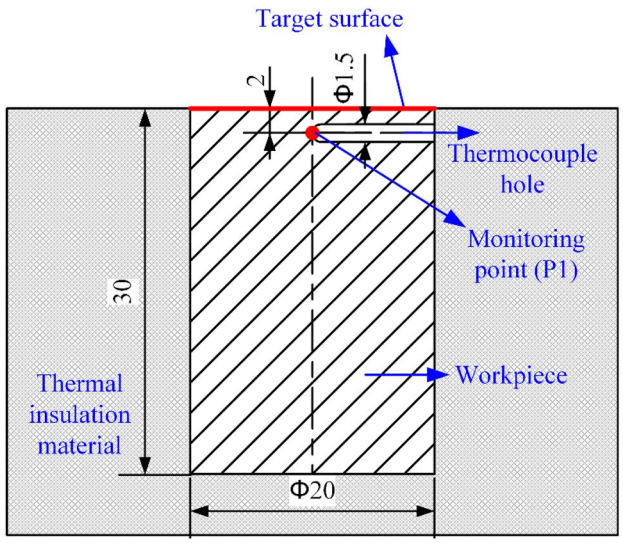

Fig. 3 Schematic diagram of the sample

device and inductor can uniformly heat the sample within 100 s. The oxide layer on the cooling surface is less due to the short heating time, and the effect of oxide layer on the interfacial heat transfer is ignored.

The data acquisition system includes temperature acquisition device and wetting front propagation acquisition device. The temperature acquisition device consists of K-type armored thermocouple, temperature recorder TC-08 and PicoLog data acquisition software. The real time voltage signal due to temperature variation from the thermocouple is acquired by USB TC-08 data acquisition device and the temperature values are shown and stored in the computer with the PicoLog application software. During the experiment, a Chronos 1.4 high-speed camera is used to record the wetting front propagation on the cooling surface, and two Godox SL-100 W LED video lights are used to provide enough light. The light intensity of LED video light can be adjustable, and it is completely flicker free from 33 to 100% output.

In order to study temperature-dependent interfacial heat transfer coefficient (T-IHTC) and the mechanism of heat transfer in the cooling process, the following experiments are carried out. When the temperature of the monitoring point reaches to 100 ℃, stop spray cooling. The experimental conditions of spray cooling are shown in Table 2. Cases 1–5 are used to investigate the effect of spray height on spray cooling. Case 3 and Cases 6–10 are used to study the effect of air pressure on spray cooling.

2.2 Uncertainty analysis

In the current study, an effort has been made to minimize the uncertainties in the experimental and computational results

Table 2 Operating conditions of spray cooling experiment

Case	Spray height (mm)	Air pressure (MPa)	Initial temperature (℃)
1	40	0.2	800
2	60	0.2	800
3	80	0.2	800
4	100	0.2	800
5	120	0.2	800
6	80	0.1	800
7	80	0.15	800
9	80	0.25	800
10	80	0.3	800

to maximize the accuracy of the research outcome. The dimensions of the specimens are determined by round steel lathe which has an accuracy of ± 0.01 mm according to the manufacturer. The main uncertainties in the results are the 'K' type thermocouples which are used to measure the real time temperature data during experimentation. The K-type thermocouples have the uncertainty of ± 0.4% full scale. The accuracy of temperature measurement is approximately ± 1.5 ℃ for K-type thermocouples. USB TC-08 data acquisition device has high resolution (20 bit) and high precision (± 0.2% reading and ± 0.5 ℃). Air pressure is obtained with an error of ± 0.01 MPa by pressure controller. And water temperature has an uncertainty of ± 0.05 ℃. Main uncertainties in this experiment are listed in Table 3.

3 Results and discussion

3.1 Inverse heat transfer analysis

The thermal analysis about predicting the surface temperature, IHTC and heat flux is an inverse heat conduction problem. Given the temperature field, solving the unknown parameters varying with time or temperature in the heat transfer process is the inverse heat conduction problem. The unknown parameters can be calculated by

Table 3 Summary of uncertainties

Parameters	Uncertainty
Dimensions of specimens	± 0.01 mm
'K' thermocouple	± 0.4%
Temperature measurement	± 1.5 ℃
USB TC-08	± 0.5 ℃
Air pressure	± 0.01 MPa
Water temperature	± 0.05 ℃

Finite Element Method or other algorithms based on the temperature field. When solving the specific heat conduction process, it is necessary to know the geometric conditions, thermophysical parameters, boundary conditions and initial conditions.

Cylindrical surface and bottom of the sample are insulated with thermal insulation material (aluminum silicate ceramic fiber paper) [17], as shown in Fig. 3. According to the definition of HTC and thermal conductivity, the HTC of thermal insulation material with the certain thickness can be approximately calculated. The HTC between sample and atmosphere is approximately equal to the ratio of thermal conductivity to thickness of the material. The thermal conductivity of thermal insulation material is 0.037–0.055 W/(m·℃) [21]. The thickness of thermal insulation material is approximately 15 mm. Then the HTC between sample and atmosphere is approximately 2.47–3.67 W/(m^2·℃). Very slow cooling rate of insulation as compare to the top surface (impinging surface) make that heat transfer approximately one dimensional and minimize the heat losses in the radial direction of the sample. Therefore, the spray cooling process is assumed to be a one-dimensional heat conduction problem when calculating surface temperature, IHTC and surface heat flux, and the validity of the one-dimensional assumption has been verified [2]. For boundary conditions, except for the top surface (impinging surface), cylindrical surface and bottom of the sample are assumed to be adiabatic.

So the heat conduction equation, initial condition and boundary conditions can be described as Eqs. (1), (2), (3) and (4), respectively.

$$\rho c_p \frac{\partial T}{\partial t} = \frac{\partial}{\partial z}(\lambda \frac{\partial T}{\partial z}) \tag{1}$$

where, T represents temperature, ℃; ρ is density, kg/m^3; c_p is specific heat capacity, J/(kg·℃); λ is thermal conductivity, W/(m °C). t is time, s. z is the coordinate along the axial direction of the sample.

$$T|_{t=0} = f(z) \tag{2}$$

$$-\lambda \frac{\partial T}{\partial z}|_{z=0} = q(t) = H(T - T_f)\ at\ the\ cooling\ surface \tag{3}$$

$$\frac{\partial T}{\partial z}|_z = 0\ at\ other\ surfaces \tag{4}$$

where, q denotes surface heat flux, W/m^2, which is a function of time t. H is the interfacial heat transfer coefficient, W/(m^2·℃), which is a function of temperature. T_f is the temperature of air-atomized water spraying, ℃.

Compared with the forward heat conduction problem, the inverse heat conduction problem uses an optimization algorithm to assume the value of the parameters required to be solved, and then substitutes the assumed value into the forward heat conduction problem. By establishing the objective function, it can judge whether the value at this time meets the requirements. If it does not meet the requirements, the optimization algorithm is needed for the next optimization. If it meets the requirements, Then the value at this time is the optimal value of the parameter requiring the solution. According to the temperature curve measured in the experiment, the surface temperature, IHTC and surface heat flux are solved by inverse heat conduction program based on the improved advance and retreat method and the golden section method [21, 22]. The flow chart of inverse heat conduction program is shown in Fig. 4. The Fortran program of the improved advance and retreat method and golden section method are shown in reference [23]. The calculation efficiency, solution accuracy and convergence of the inverse heat conduction program have been verified in references [21, 24].

3.2 Effects of spray height and air pressure on IHTC

3.2.1 Effects of spray height on IHTC

Spray height is the distance between the atomizer and the target surface. The atomizer-to-surface has essential influence on the IHTC during the air-atomized water spray cooling [25]. The temperatures of P1 point under the different spray height recorded by USB TC-08 are shown in Fig. 5, while the surface temperature and IHTC curves which calculated by the IHCM [21, 22] are shown in Figs. 6 and 7, respectively. It can be seen from Fig. 6 that when the air pressure remains constant (0.2 MPa), the cooling rate increases with the decreases of spray height.

It can be seen from Fig. 7 that when the air pressure is constant, as the spray height decreases, the IHTC increases. When the spray height is between 80—120 mm, the surface temperature decreases from 800 ℃ to 700 ℃ during the spray cooling process, the IHTC gradually increases, reaching about 2000 W/(m^2·℃). During the spray cooling process where the surface temperature drops from 700 ℃ to 400 ℃, the slope of IHTC curve is basically 0, and the IHTC remains almost unchanged. When the surface temperature is below 400 ℃, the IHTC increases continuously during spray cooling. When the spray height is 120 mm, 100 mm, 80 mm, the maximum IHTC is about 10,000 W/(m^2·℃), 11,000 W/(m^2·℃), 12,500 W/(m^2·℃), respectively. When the spray height is 60 mm, the surface temperature is reduced from 800 ℃ to about 425 ℃, the IHTC gradually increases, can reach about 3000 W/(m^2·℃). During the spray cooling of the surface temperature below 425 ℃, the slope of the IHTC is increased, and the IHTC is increased. The maximum IHTC can reach about 13,000 W/(m^2·℃). When the spray height

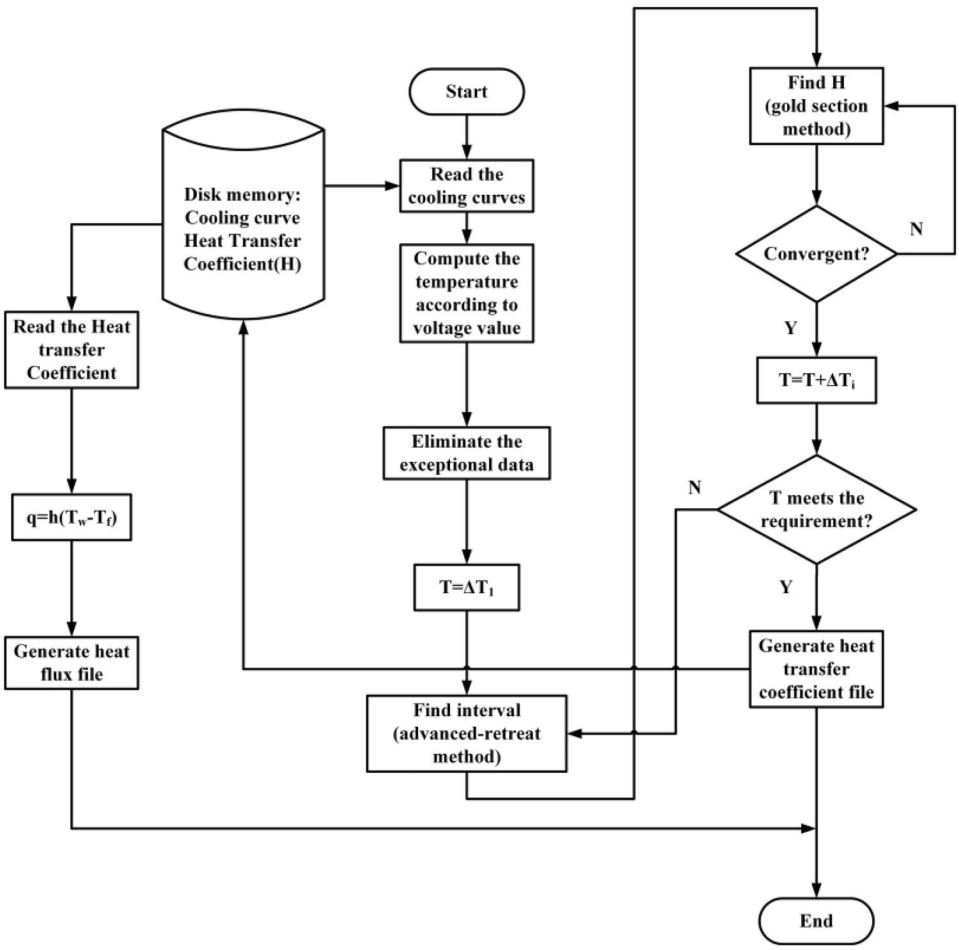

Fig. 4 Flow chart of the inverse heat conduction program

is 40 mm, the surface temperature is reduced from 800 ℃ to about 500 ℃, the IHTC gradually increases. During the spray cooling of the surface temperature below 500 ℃, the IHTC has increased. The maximum IHTC can reach approximately 14,500 W/(m^2·℃). In conclusion, when the spray height goes up, the droplets impact energy decreases, which

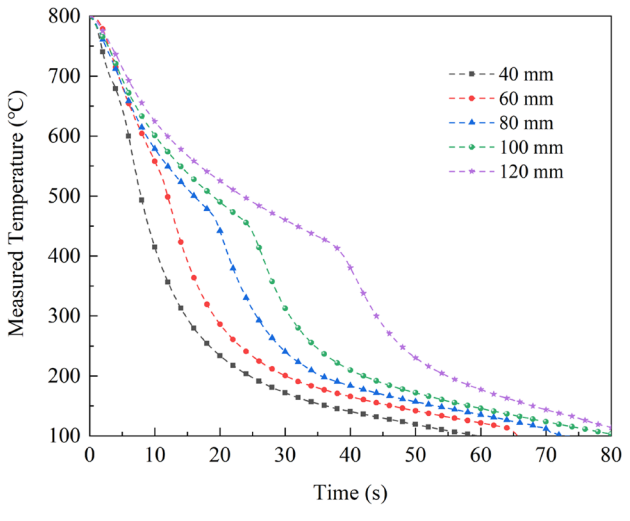

Fig. 5 Temperature curves at the monitoring point P1 for the samples with the different spray heights (Measured by the thermocouple in the experiment)

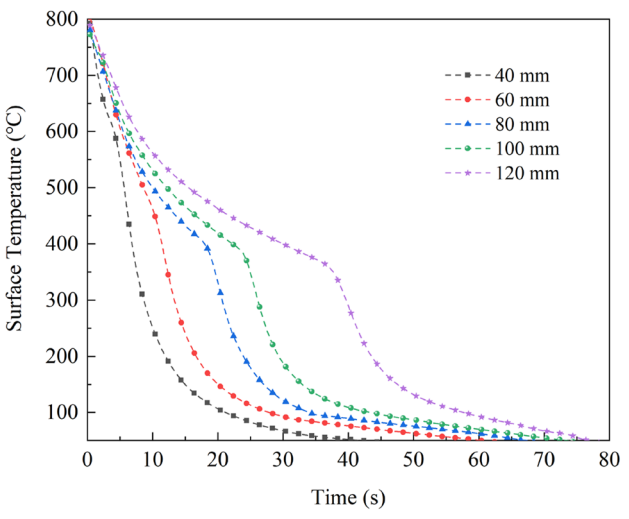

Fig. 6 Temperature curves on the cooling surface for the samples with the different spray heights (Calculated by the IHCM)

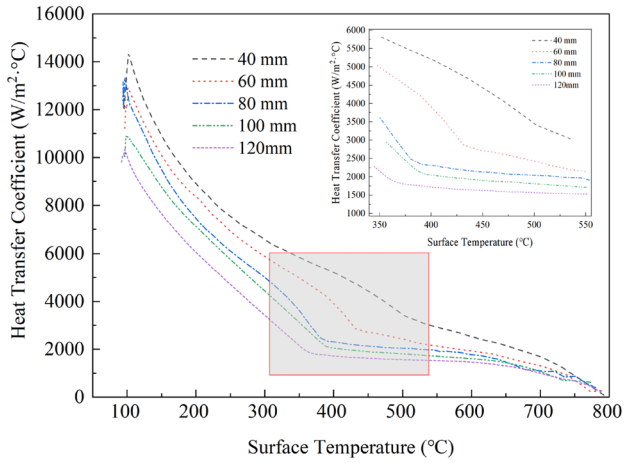

Fig. 7 IHTC on the cooling surface of sample for the different spray height

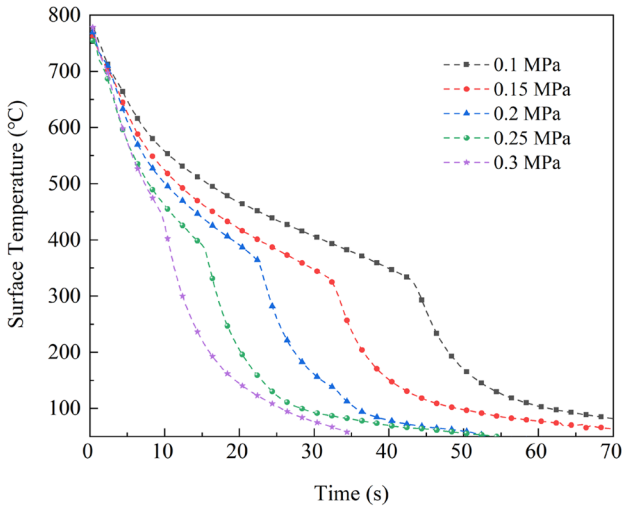

Fig. 9 Temperature curves on the cooling surface for the samples with the different air pressure

disables the positive effect of the increased impinged cooling area and accordingly decreases the IHTC [10].

3.2.2 Effects of air pressure on IHTC

Air pressure is also one of the most important factors to affect the IHTC. The air pressure was 0.1 MPa, 0.15 MPa, 0.2 MPa, 0.25 MPa and 0.3 MPa, respectively. The temperature curves at the monitoring point P1 recorded by USB TC-08 are shown in Fig. 8. The surface temperature and IHTC calculated by the IHCM [21, 22] are shown in Figs. 9 and 10, respectively. When the spray height and initial temperature are constant, the time required for the cooling surface to cool to a certain temperature decreases as the air pressure increases. When the spray pressure is 0.3 MPa, 0.25 MPa, 0.2 MPa, 0.15 MPa, 0.1 MPa, the cooling time to 100 ℃ is about 57 s, 65 s, 70 s, 82 s, 90 s, respectively. The greater the air pressure, the faster the cooling rate.

(Calculated by the IHCM).

As can be seen from Fig. 10, when the air pressure is between 0.1—0.3 MPa, the surface temperature is reduced from 800 ℃ to about 700 ℃, the IHTC gradually increases, reaches about 1000 W/(m^2·℃). When the air pressure is 0.1 MPa, the surface temperature is reduced from 700 ℃ to about 330 ℃, the slope of the IHTC curve is small, and the IHTC increases slowly. As the surface temperature is about 330 ℃, the IHTC reaches about 2000 W/(m^2·℃). During the spray cooling process below about 330 ℃, the IHTC

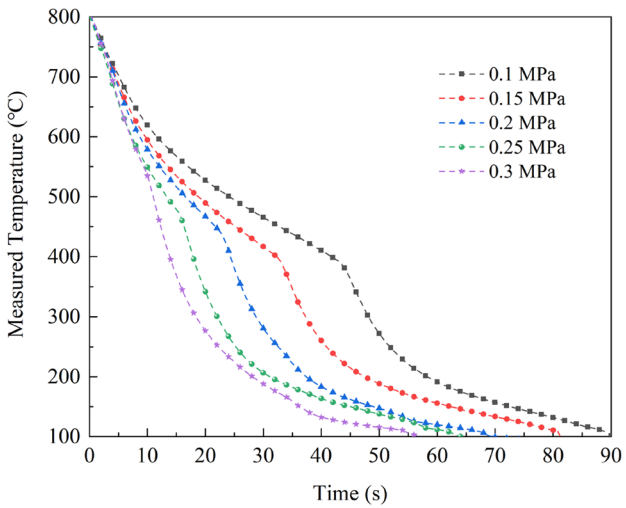

Fig. 8 Temperature curves of monitoring point P1 for the samples with the different air pressure (Measured by the thermocouple)

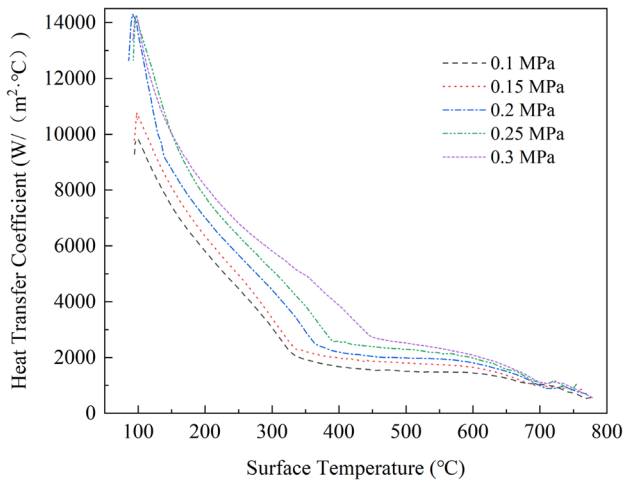

Fig. 10 IHTC on the cooling surface of samples at different air pressures

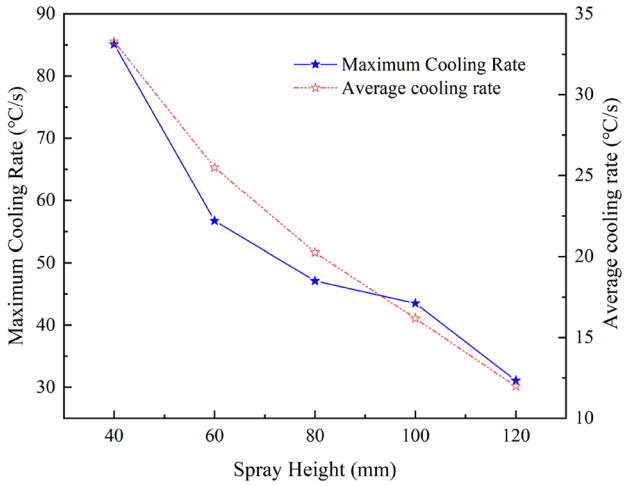

Fig. 11 Cooling rate at the different spray heights

has increased, the maximum value of the IHTC is about 10,000 W/(m^2·℃). When the air pressure is 0.3 MPa, the surface temperature is reduced from 700 ℃ to about 450 ℃. The slope of the IHTC is small, and the IHTC increases slowly. When the surface temperature is about 450 ℃, the IHTC reaches about 3000 W/(m^2·℃). During the spray cooling process of less than about 450 ℃, the IHTC has increased, the maximum value of the IHTC is about 14,000 W/(m^2·℃). When the spray height is constant, increase the air pressure, the number of droplets that is atomized is increased, and the droplet kinetic energy is increased, the impact of the cooling surface is large, the heat transfer efficiency is improved, and the IHTC is increased.

3.3 Effects of spray height and air pressure on cooling rate

3.3.1 Effects of spray height on cooling rate

When studying the effect of the spray height on the cooling rate, the air pressure is set to be 0.2 MPa. The tangent slope of temperature curve shown in Fig. 6 is the cooling rate on the cooling surface. The parameter ΔT/Δt characterizes a rate of the temperature change during the time interval corresponding to the sample rate of the thermocouple inside the hole. The maximum cooling rate is the maximum value of the parameter ΔT/Δt during the spray cooling process where the surface temperature is cooled from 800 ℃ to 100 ℃. The average cooling rate is the mean of the parameter ΔT/Δt during the spray cooling process where the surface temperature is cooled from 800 ℃ to 100 ℃. As the spray height is 40 mm, the maximum cooling rate is approximately 85.1 ℃/s, and the average cooling rate is approximately 33.3 ℃/s. As the spray height is 120 mm, the maximum cooling rate is approximately 31.1 ℃/s, and the average cooling rate is approximately 12.0 ℃/s, as shown in Fig. 11.

According to the experiment of air-atomized water spray cooling process, the spray cone angle is smaller. When the atomizer is closer to the target surface, the cooling surface is not completely covered inside the spray cone, the actual spray area is reduced, and the cooling effect is declined. However, the loss of droplet kinetic energy is small. The droplet has a large momentum and has a strong impact on the cooling surface, the surface liquid film is quickly destroyed and the cooling rate is faster. While the spray height is high, part of the sprayed atomized droplets will fall outside the target surface, the number of splashed droplets will increase, the effective flow rate actually sprayed to the surface will be reduced, and the impact of the droplets will be smaller. Therefore, the cooling rate is slower.

3.3.2 Effects of air pressure on cooling rate

When studying the effect of the air pressure on the cooling rate, the spray height is constant (80 mm). As the air pressure is 0.1 MPa, the maximum cooling rate is approximately 32.8 ℃/s, the average cooling rate is approximately 11.1 ℃/s. As the air pressure is 0.3 MPa, the maximum cooling rate is approximately 62.6 ℃/s, and the average cooling rate is approximately 26.6 ℃/s, as shown in Fig. 12.

As the air pressure increases, the initial velocity of the droplets and the number or density of the droplets increase, while the size of droplets decreases, which is conductive to penetrating the liquid film and enhancing the disturbance to the liquid film. The radial velocity component of the liquid droplet on the heat exchange wall becomes larger, which makes the elimination speed of the liquid film on the heating surface faster, that is, the erosion effect of the liquid film on

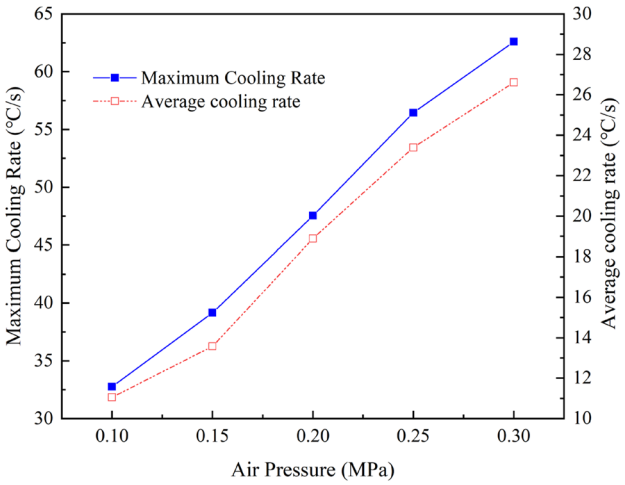

Fig. 12 Cooling rate at different air pressures

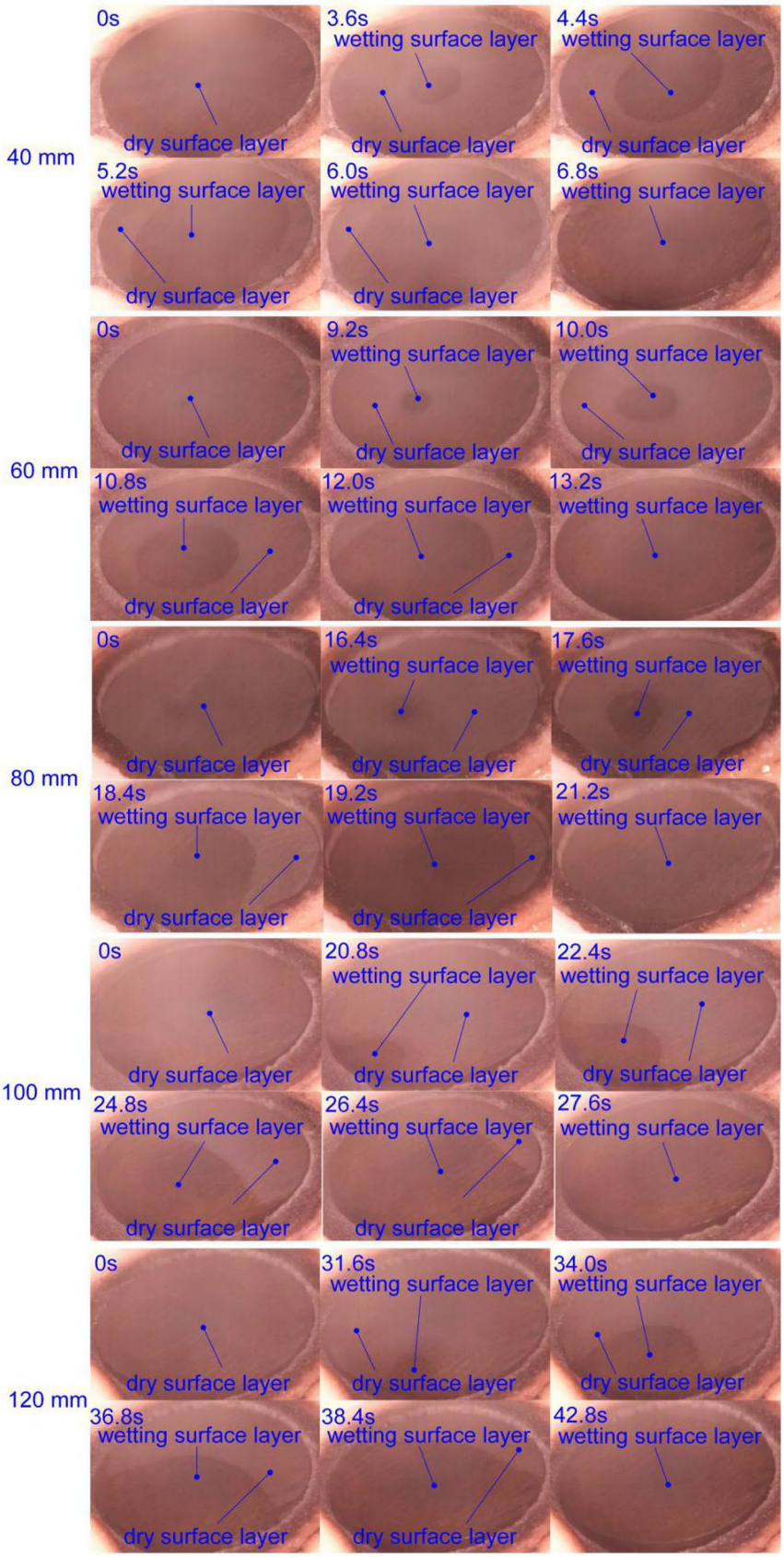

Fig. 13 Wetting front propagation on the hot metallic surface of samples for the different spray heights (40 mm, 60 mm, 80 mm, 100 mm and 120 mm)

the wall surface is enhanced, and the heat transfer effect is improved.

3.4 Effects of spray height and air pressure on wetting front propagation

3.4.1 Effects of spray height on wetting front propagation

The Chronos 1.4 high-speed camera is used to record the wetting front propagation on the target surface of sample in the cooling process. The wetting front propagation on the hot metallic surface for the different spray heights is shown in Fig. 13.

It can be clearly seen from Fig. 13 that there are three surface states on the target surface during the air-atomized water spray cooling. One is heat transfer with a dry surface layer, the other is heat transfer with a wetting surface layer, and another is heat transfer with the transition state, which is the state between the dry surface layer and the wetting surface layer. At the beginning of the transition state stage, the liquid film may begin to appear on any position of the hot metallic surface, and gradually expands.

until it covers the whole surface. According to the wetting front propagation taken by the high-speed camera and the surface temperature calculated by the IHCM, the retention time of the three states can be determined.

The retention time of the dry surface layer is different for the different spray heights during the air-atomized water spray cooling. When the spray heights are 40 mm, 60 mm, 80 mm, 100 mm and 120 mm, the retention time of the dry surface layer are approximately 3.6 s, 9.2 s, 16.4 s, 20.8 s and 31.6 s, respectively, as depicted in Fig. 14(a). The corresponding surface temperatures at the end of the dry surface layer are about 617.4 ℃, 484.6 ℃, 417.3 ℃, 411.7 ℃ and 390.5 ℃, respectively. This temperature is the lowest temperature to maintain the stability of the vapor film, called Leidenfrost Point (LFP), as shown in Fig. 14(b). The LFP temperature decreases with the increasing of the spray height.

Some tiny water droplets are quickly vaporized when they encounter the hot metallic surface. A lot of steam bubbles are formed on the hot metallic surface. The heat exchange between the hot metallic surface and air-atomized water spray cooling is mainly by the evaporation of water droplets, this process is evaporation. As more and more water droplets dropped on the hot metallic surface, the steam bubble bursts and form a vapor film, as shown in Fig. 15. The vapor film leads to the poor heat transfer effectiveness between the high metallic surface and the air-atomized water spray [26]. The droplets float on the vapor film and evaporates very slowly. This process is called as film boiling, which the surface temperature is above the Leidenfrost temperature [6]. Film boiling is dominated by formation of a vapor layer along

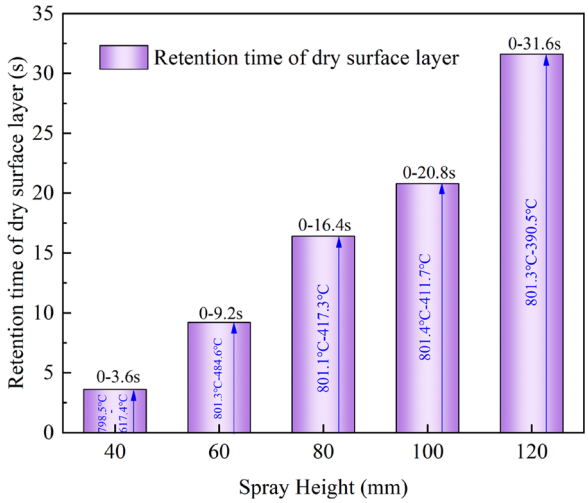

(a) The retention time of dry surface layer at different spray heights

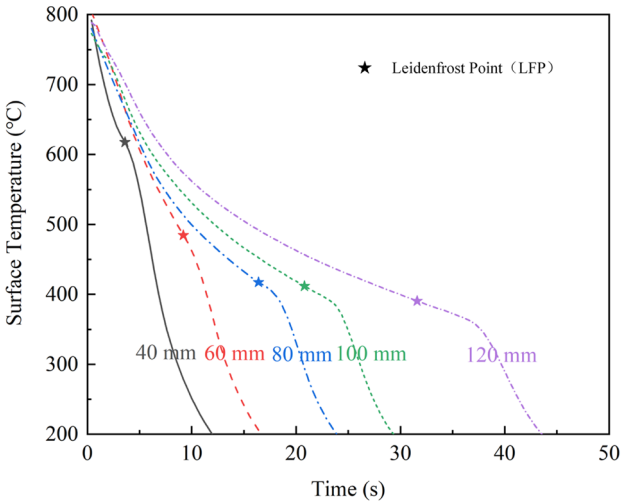

(b) Leidenfrost Point (LFP) under different spray heights

Fig. 14 The maintenance time of dry surface layer and Leidenfrost Point. (**a**) The retention time of dry surface layer at different spray heights, (**b**) Leidenfrost Point (LFP) under different spray heights

the entire hot metallic surface. Because of the low thermal conductivity of vapor, cooling rate in film boiling is quite slow [27]. It is worth pointing out that there is no film boiling when the spray height is 40 mm. This is because when the spray height goes down, the perpendicular velocity of droplets increases. High kinetic energy droplet and fast flow can easily blow away the vapor layer on the hot metallic surface, leading to the decrease of the percentage of film boiling, and the film boiling stage can easily be replaced by the evaporation and convection between the air-atomized water spray and the hot metallic surface [28], as shown in Fig. 15.

After the LFP temperature, the surface state changes to the transition state [29, 30], and the heat transfer efficiency is enhanced. The retention time of transition state is approximately 3.2 s, 4 s, 4.8 s, 6.8 s and 11.2 s, respectively, as

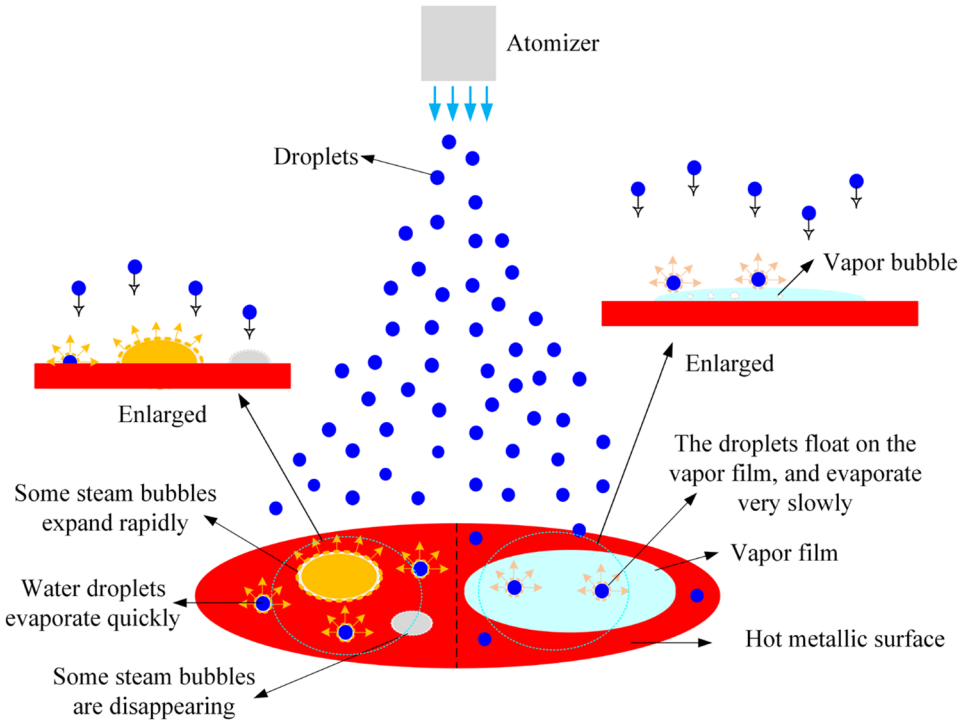

Fig. 15 Evaporation and film boiling process of water droplets sprayed on the hot metallic surface

shown in Fig. 16. At this stage, the surface temperature ranges are 617.4—402.6 ℃, 484.6—305.3 ℃, 417.3—277.0 ℃, 411.7—244.0 ℃ and 390.5—214.4 ℃, respectively. The retention time of the transition state increases with the increasing of the spray height.

At this stage, the vapor film becomes more and more unstable until the critical heat flux (CHF) is reached [29].

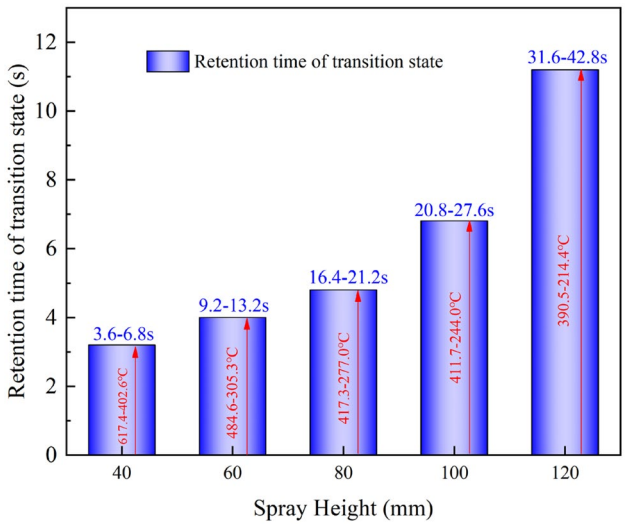

Fig. 16 The retention time of transition state for the different spray heights

The vapor film begins to crack from an uncertain position on the hot metallic surface, some discontinuous bubbles are formed on the surface. The discontinuous bubbles can make some tiny droplets contact the hot metallic surface. As lots of droplets impinge on the surface, some droplets rebound from the hot metallic surface, some droplets deposit on the hot metallic surface, and parts of droplets splash when others depositing on the hot metallic surface. The droplets deposited on the hot metallic surface form the wetting surface layer. The vapor bubbles are washed away by the droplets splashed, and a lot of heat energy is taken away, as shown in Fig. 17. The IHTC increases, as shown in Fig. 7. This process is called as the transition boiling. At the lower temperature boundary of the transition boiling regime, where the entire surface becomes available for wetting and heat transfer rate reaches a maximum (so called CHF) [31].

After the transition boiling, it is nucleate boiling until the surface temperature drops to the boiling temperature of water (100 ℃). At this process, the whole surface was covered by water droplets, and a complete liquid film is formed. The nucleate boiling regime is marked by abundance of vapor bubbles nucleating, growing, and departing from the surface at high frequency [27], as shown in Fig. 18. Evaporation of the liquid film on the liquid–vapor layer interface was induced by convective and radiative heat transfer through the vapor layer [12].

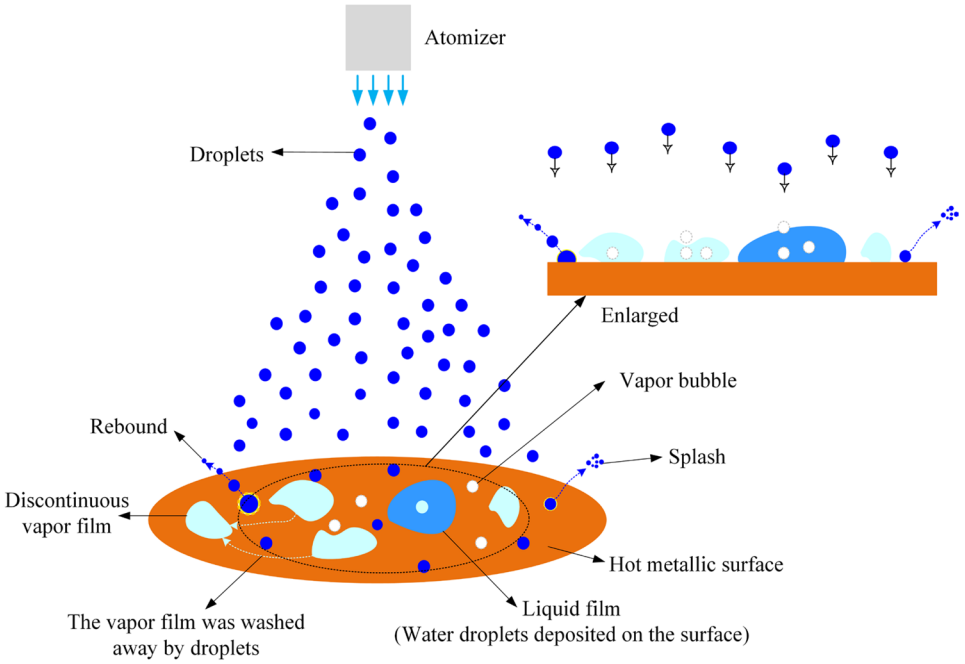

Fig. 17 Transition boiling

3.4.2 Effects of air pressure on wetting front propagation

The wetting front propagation under the different pressure taken by the Chronos 1.4 high-speed camera is shown in Fig. 19. It can be clearly seen from Fig. 19 that there are also three surface states (dry surface layer, transition state, wetting surface layer) on the target surface during the air-atomized water spray cooling. According to the wetting front propagation taken by the high-speed camera and the surface temperature calculated by the IHCM, the retention time of different states is analyzed. (0.1 MPa, 0.15 MPa, 0.2 MPa, 0.25 MPa and 0.3 MPa).

The maintenance time and temperature range of the different states are shown in Fig. 20. As the air pressures are 0.1 MPa, 0.15 MPa, 0.2 MPa, 0.25 MPa and 0.3 MPa, the retention time of the dry surface layer are approximately 40.0 s, 29.6 s, 20.0 s, 13.6 s and 8.4 s, respectively, as depicted in Fig. 20. When the temperature drops to about 349.4 ℃, 350.1 ℃, 391.0 ℃, 408.2 ℃ and 474.3 ℃, respectively, the surface state changes to transition state. This temperature is the LFP temperature. The LFP temperature

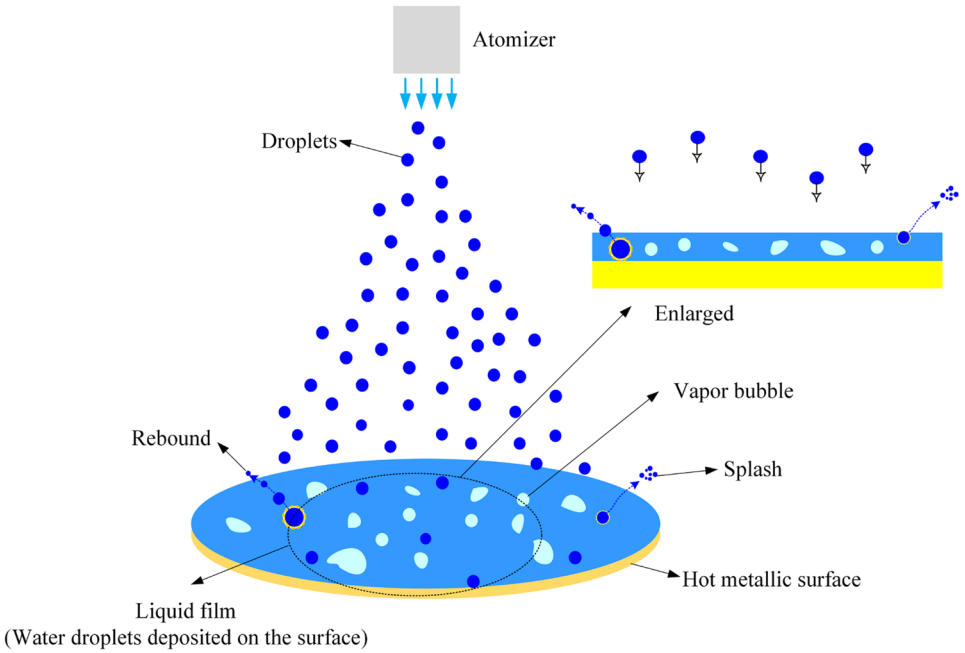

Fig. 18 Nucleate boiling

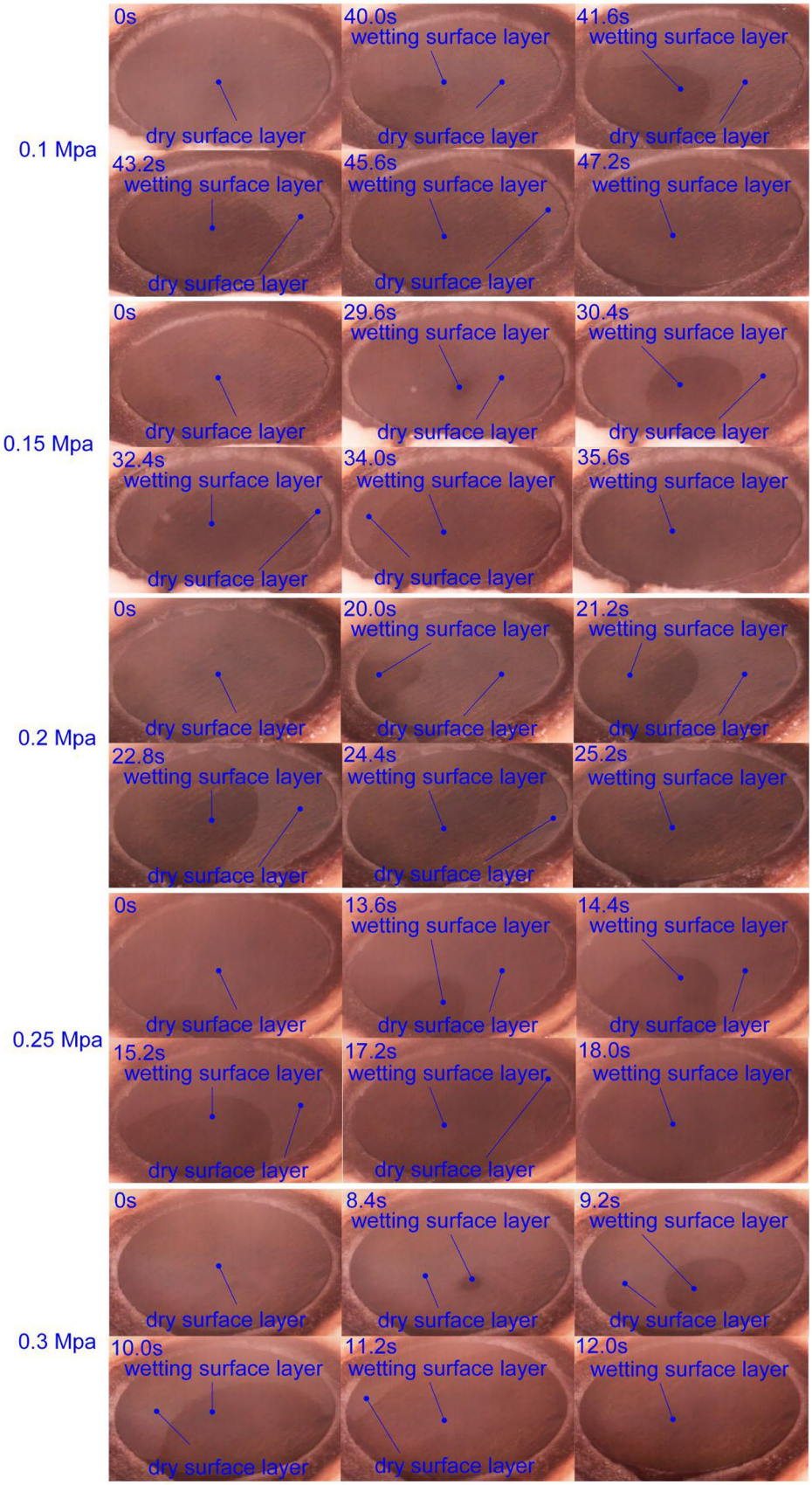

Fig. 19 Wetting layer evolution of sample surface for the different air pressure

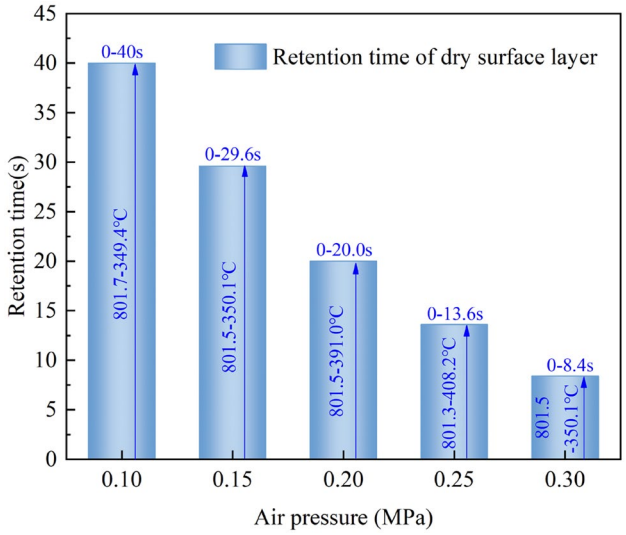

Fig. 20 The retention time and the temperature range of the dry surface layer at different air pressures

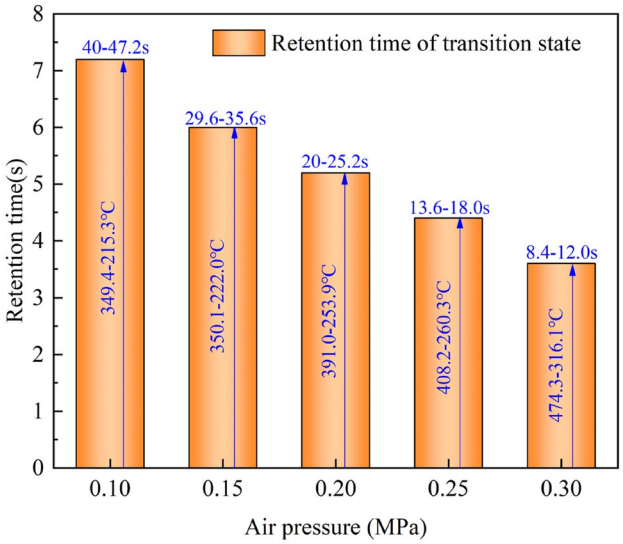

Fig. 22 The retention time and the temperature range of the transition state at different air pressures

under the different air pressures is shown in Fig. 21. The LFP temperature increases with the increase of the air pressure. When the air pressure increases by 0.1 MPa, the LFP temperature changes approximately 50 ℃. After the LFP temperature, the surface state is the transition state. During the transition state, the retention time under the different air pressures is 7.2 s, 6.0 s, 5.2 s, 4.4 s and 3.6 s, respectively. The surface temperature ranges of the transition state are 349.4—215.3 ℃, 350.1—222.0 ℃, 391.0—253.9 ℃, 408.2—260.3 ℃ and 474.3—316.1 ℃, respectively, as shown in Fig. 22.

Just like the air-atomized water spray cooling under the different spray heights, the working fluid is atomized into a large number of smaller and colder droplets, and then impinged on the hot metallic surface, which removes a lot of heat through the ways of convection and evaporation. Obviously, the steam layer can be seen through the pictures taken by the Chronos 1.4 high-speed camera. When the air pressure is relatively low, the effect of air assist is not obvious. The number of droplets which are atomized is small. After the vapor film is formed, it is hard to be broken. Therefore, the time of dry surface layer remains longer at low air pressure. However, when the air pressure increases, the droplets produced by the air-assisted atomizer become more and more. The vapor film on the hot metallic surface is washed away by droplets. Nevertheless, when the air pressure becomes larger, the film boiling stage and transitional boiling time become shorter. Maybe, when the air pressure becomes larger and larger, the film boiling regime does not exist.

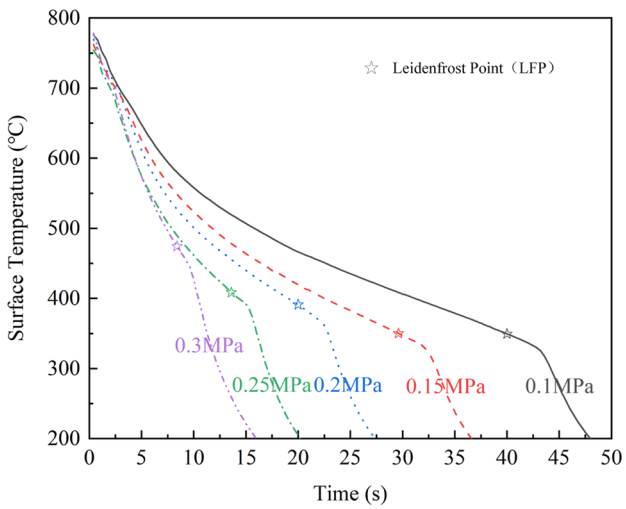

Fig. 21 LFP temperature under different air pressures

4 Conclusion

In this paper, the results of experimental investigation on thermal characteristics of spray cooling of hot surface under controlled parameters have been reported. The cooling rate and heat transfer coefficient were discussed for different spray height and air pressure. The conclusions are as follows:

1. The spray height and air pressure all have significant influence on IHTC in air-atomized water spray cooling. These factors affect the boiling state on the hot metallic surface by influence the condition of the flow field during the air-atomized water spray cooling. When the

spray height is 40 mm, there is no film boiling on the target surface.

2. During the air-atomized water spray cooling, the liquid–solid IHTC between the hot metallic surface and spray medium changes with air pressure and spray height. IHTC is positive proportional to the air pressure and inversely proportional to the spray height.
3. It has also been noticed that cooling rate is affected by air pressure and spray height. The cooling rate shows an increasing trend with an increasing air pressure because of the formation of a large number of atomized droplets. In addition, it is also observed that the cooling rate decreases with increasing spray height.
4. The retention time of the dry surface layer and the transition state is proportional to spray height and inversely proportional to air pressure. The LFP point decreases with the increasing of the spray height and increases with the increasing of the air pressure. Moreover, spray height has a greater effect on the LFP point than air pressure.

Acknowledgements This work was financially supported by the National Natural Science Foundation of China (51575324, 52005304), Natural Science Foundation of Shandong Province (2019GGX104009).

Declarations

Conflict of interest The authors declare that they have no known competing financial interests or personal relationships that could have appeared to influence the work reported in this paper.

References

1. Waldeck S, Woche H, Specht E, Fritsching U (2018) Evaluation of heat transfer in quenching processes with impinging liquid jets. Int J Therm Sci 134:160–167. https://doi.org/10.1016/j.ijthermalsci.2018.08.001
2. Dou R, Wen Z, Zhou G et al (2014) Experimental study on heat-transfer characteristics of circular water jet impinging on high-temperature stainless steel plate. Appl Therm Eng 62:738–746. https://doi.org/10.1016/j.applthermaleng.2013.10.037
3. Das L, Pati AR, Panda A et al (2020) The enhancement of spray cooling at very high initial temperature by using dextrose added water. Int J Heat Mass Transf 150:119311. https://doi.org/10.1016/j.ijheatmasstransfer.2020.119311
4. Uusikallio S, Koskenniska S, Ilmola J et al (2020) Determination of effective heat transfer coefficient for water spray cooling of steel. Procedia Manuf 50:488–491. https://doi.org/10.1016/j.promfg.2020.08.088
5. Khangembam C, Singh D, Handique J, Singh K (2020) Experimental and numerical study of air-water mist jet impingement cooling on a cylinder. Int J Heat Mass Transf 150:119368. https://doi.org/10.1016/j.ijheatmasstransfer.2020.119368
6. Chabicovsky M, Kotrbacek P, Bellerova H et al (2020) Spray cooling heat transfer above leidenfrost temperature. Metals (Basel) 10:1–16. https://doi.org/10.3390/met10091270
7. Pati AR, Lily BAP et al (2017) Enhancement of heat removal rate of high mass flux spray cooling by sea water. Exp Therm Fluid Sci 89:19–40. https://doi.org/10.1016/j.expthermflusci.2017.07.012
8. Kim J (2007) Spray cooling heat transfer: The state of the art. Int J Heat Fluid Flow 28:753–767. https://doi.org/10.1016/j.ijheatfluidflow.2006.09.003
9. Mohapatra SS, Jha JM, Srinath K et al (2014) Enhancement of cooling rate for a hot steel plate using air-atomized spray with surfactant-added water. Exp Heat Transf 27:72–90. https://doi.org/10.1080/08916152.2012.719068
10. Nayak SK, Mishra PC (2016) Thermal characteristics of air-water spray impingement cooling of hot metallic surface under controlled parametric conditions. J Therm Sci 25:266–272. https://doi.org/10.1007/s11630-016-0859-6
11. Sardar R, Bachhar P, Majumder S (2020) Air-water mist cooling characteristics of an MS plate in a Laboratory scale ROT- an Experimental Observation. International Conference on Advances in Material Science & Mechanical Engineering [ICAMSME 2020]
12. Silk EA, Golliher EL, Selvam RP (2008) Spray cooling heat transfer: Technology overview and assessment of future challenges for micro-gravity application. Energy Convers Manag 49:453–468. https://doi.org/10.1016/j.enconman.2007.07.046
13. Zhao X, Yin Z, Zhang B, Yang Z (2020) Experimental investigation of surface temperature non-uniformity in spray cooling. Int J Heat Mass Transf 146:118819. https://doi.org/10.1016/j.ijheatmasstransfer.2019.118819
14. Chakraborty S, Sarkar I, Roshan A et al (2019) Spray cooling of hot steel plate using aqueous solution of surfactant and polymer. Therm Sci Eng Prog 10:217–231. https://doi.org/10.1016/j.tsep.2019.02.003
15. Ma H, Silaen A, Zhou C (2020) Numerical Development of Heat Transfer Coefficient Correlation for Spray Cooling in Continuous Casting. Front Mater 7:1–18. https://doi.org/10.3389/fmats.2020.577265
16. Dou R, Wen Z, Zhou G (2015) Heat transfer characteristics of water spray impinging on high temperature stainless steel plate with finite thickness. Int J Heat Mass Transf 90:376–387. https://doi.org/10.1016/j.ijheatmasstransfer.2015.06.079
17. Zhang X, Wen Z, Dou R et al (2014) Experimental study of the air-atomized spray cooling of high-temperature metal. Appl Therm Eng 71:43–55. https://doi.org/10.1016/j.applthermaleng.2014.06.026
18. Ondrouskova J, Pohanka M, Vervaet B (2013) Heat-flux computation from measured-temperature histories during hot rolling. Mater Tehnol 47:85–87
19. Komínek J, Pohanka M (2016) Estimation of the number of forward time steps for the sequential Beck approach used for solving inverse heat-conduction problems. Mater Tehnol 50:207–210. https://doi.org/10.17222/mit.2014.192
20. Hadała B, Malinowski Z, Telejko T et al (2019) Experimental identification and a model of a local heat transfer coefficient for water – Air assisted spray cooling of vertical low conductivity steel plates from high temperature. Int J Therm Sci 136:200–216. https://doi.org/10.1016/j.ijthermalsci.2018.10.026
21. Li H, He L, Zhang C, Cui H (2015) Research on the effect of boundary pressure on the boundary heat transfer coefficients between hot stamping die and boron steel. Int J Heat Mass Transf 91:401–415. https://doi.org/10.1016/j.ijheatmasstransfer.2015.07.102
22. Huiping L, Guoqun Z, Shanting N, Yiguo L (2006) Inverse heat conduction analysis of quenching process using finite-element and optimization method. Finite Elem Anal Des 42:1087–1096. https://doi.org/10.1016/j.finel.2006.04.002
23. Zou L, Ning L, Wang X et al (2021) Evaluation of interfacial heat transfer coefficient based on the experiment and numerical simulation in the air-cooling process. Heat Mass Transf. https://doi.org/10.1007/s00231-021-03113-x

24. Li H, Zhao G, He L, Mu Y (2008) High-speed data acquisition of the cooling curves and evaluation of heat transfer coefficient in quenching process. Meas J Int Meas Confed 41:676–686. https://doi.org/10.1016/j.measurement.2007.10.003
25. Cebo-Rudnicka A, Malinowski Z, Buczek A (2016) The influence of selected parameters of spray cooling and thermal conductivity on heat transfer coefficient. Int J Therm Sci 110:52–64. https://doi.org/10.1016/j.ijthermalsci.2016.06.031
26. Guo R, Wu J, Liu W et al (2016) Investigation of heat transfer on 2024 aluminum alloy thin sheets by water spray quenching. Exp Therm Fluid Sci 72:249–257. https://doi.org/10.1016/j.expthermflusci.2015.11.014
27. Cai C, Mudawar I, Liu H, Si C (2020) Theoretical Leidenfrost point (LFP) model for sessile droplet. Int J Heat Mass Transf 146:118802. https://doi.org/10.1016/j.ijheatmasstransfer.2019.118802
28. Ying L, Gao T, Dai M et al (2017) Experimental investigation of temperature-dependent interfacial heat transfer mechanism with spray quenching for 22MnB5 steel. Appl Therm Eng 121:48–66. https://doi.org/10.1016/j.applthermaleng.2017.04.029
29. Wendelstorf J, Spitzer KH, Wendelstorf R (2008) Spray water cooling heat transfer at high temperatures and liquid mass fluxes. Int J Heat Mass Transf 51:4902–4910. https://doi.org/10.1016/j.ijheatmasstransfer.2008.01.032
30. Liang G, Mudawar I (2017) Review of drop impact on heated walls. Int J Heat Mass Transf 106:103–126. https://doi.org/10.1016/j.ijheatmasstransfer.2016.10.031
31. Hsieh SS, Fan TC, Tsai HH (2004) Spray cooling characteristics of water and R-134a. Part II: Transient cooling. Int J Heat Mass Transf 47:5713–5724. https://doi.org/10.1016/j.ijheatmasstransfer.2004.07.023